Table S1 Comparison of the access channel residues of CYP108D1 and CYP108A1. Differences in CYP108D1 are underlined.

CYP108D1	**CYP108A1**
Val80	Ile78
Thr82	Tyr80
Gly86	Asn84
Ala90	Met88
Leu100	Val98
Phe190	Phe188

Table S2 Comparison of the active site residues of CYP108D1 and CYP108A1. Differences in CYP108D1 are underlined.

N. aromaticivorans **CYP108D1**	**Pseudomonas sp. CYP108A1 (P450terp)**
Thr79	Glu77
Val101	Ile99
Ser103	Ser101
Val105	Thr103
Gln106	Ser104
Phe190	Phe188
Ile265	Ala263
Ser268	Thr266
Ala269	Ala267
Asp272	Asp270
Thr273	Thr271
Val316	Val314
Phe319	Phe317
Phe416	Phe414
Val417	Val415

Table S3 CYP108D1-phenylcyclohexane interactions from the docking results.

The first mode	phenyl ring	C1	Phe416Cε2(4.1 Å), Ile265δ1(4.4 Å)
		C2	Phe416Cζ(4.2 Å), Ile265δ1(3.9 Å), Val105 Cγ1(3.7 Å)
		C3	Phe416Cζ(3.7 Å), Phe319Cζ(4.0 Å), Val105Cγ1(3.7 Å), Ile265δ1(3.6 Å)
		C4	Ile265δ1(3.9 Å), Phe416Cζ(3.8 Å), Phe416Cε2(3.8 Å)
		C5	Ile265δ1(4.3 Å), Phe416Cε2(3.7 Å)
		C6	Phe190Cδ2(4.3 Å), Phe416Cε2(3.9 Å), Phe190Cγ(4.3 Å), Phe190Cβ(4.3 Å)
	aliphatic cyclohexyl ring	C1	Ala269Cα(3.4 Å), Ala269Cβ(3.4 Å), Phe416Cζ(4.1 Å)
		C2	Ala269Cα(3.6 Å), Thr273Cγ2(4.1 Å), Val417Cγ2(4.0 Å), Phe416Cε2(3.8 Å)
		C3	Ala269Cα(4.4 Å), Thr273Cγ2(3.4 Å), Val316Cγ2(3.3 Å), Val417Cγ2(3.8 Å), Phe416Cζ(3.8 Å)
		C4	Ala269Cα(3.9 Å), Thr273Cγ2(3.6 Å), Val316Cγ2(3.5 Å)
		C5	Ala269Cβ(3.4 Å), Phe319Cζ(4.2 Å), Phe319Cε2(4.3 Å)
		C6	Ala269Cβ(3.7 Å), Phe319Cζ(3.5 Å), Phe416Cζ(4.2 Å),

The second mode	phenyl ring	C1	Phe190Cβ(4.1 Å), Phe416Cε2(4.3 Å), Val417Cγ2(4.4 Å)
		C2	Phe190Cβ(3.8 Å), Ser268Cβ(3.8 Å), Phe416Cε2(3.8 Å)
		C3	Phe416Cε2(3.5 Å), Phe416Cζ(4.1 Å)
		C4	Ala269Cα(3.8 Å), Phe416Cε2(3.7 Å), Val417Cγ2(3.8 Å)
		C5	Thr273Cγ2(3.9 Å), Val417Cγ2(3.2 Å)
		C6	Asp272Cβ(4.3 Å), Val417Cγ1(4.2 Å), Val417Cγ2(3.5 Å)
	aliphatic cyclohexyl ring	C1	Ala269Cα(3.2 Å), Thr273Cγ2(4.1 Å), Phe416Cε2(4.2 Å), Phe416Cζ(4.1 Å), Val417Cγ2(4.2 Å)
		C2	Thr273Cγ2(3.4 Å), Val316Cγ2(3.5 Å), Phe416Cε2(4.0 Å), Phe416Cζ(3.7 Å), Val417Cγ2(3.5 Å)
		C3	Val316Cγ1(3.5 Å), Val316Cγ2(3.4 Å), Phe319Cζ(3.4 Å), Phe319Cε2(3.5 Å), Phe416Cζ(3.3 Å)
		C4	Val316Cγ1(4.5 Å), Val316Cγ2(4.2 Å), Phe319Cζ(3.4 Å), Phe319Cε2(3.5 Å)
		C5	Ala269Cβ(3.4 Å), Ile265δ1(4.5 Å), Phe319Cζ(3.8 Å)
		C6	Ala269Cα(3.7 Å), Ala269Cβ(3.7 Å), Ile265δ1(4.5 Å), Phe319Cζ(4.3 Å), Phe416Cε2(4.1 Å), Phe416Cζ(3.9 Å)

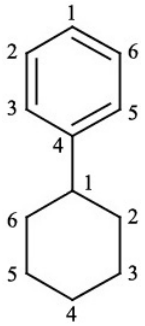

Table S4 CYP108D1-phenanthrene interactions from the docking results.

C1	Ala269Cα(3.6 Å), Thr273Cγ2(3.2 Å), Val316Cγ2(3.8 Å), Val417Cγ2(4.0 Å)
C2	Ala269Cα(4.0 Å), Thr273Cγ2(3.6 Å), Val316Cγ2(3.4 Å)
C3	Ala269Cβ(3.7 Å), Phe319Cζ(3.9 Å), Phe319Cε2(4.0 Å)
C4	Ala269Cβ(3.6 Å), Phe319Cζ(3.6 Å)
C5	Ala269Cα(3.7 Å), Ala269Cβ(3.6 Å), Phe319Cζ(4.1 Å), Phe416Cζ(3.9 Å)
C6	Ala269Cα(3.4 Å), Phe416Cε2(4.0 Å), Phe416Cζ(3.9 Å)
C7	Ala269Cα(3.8 Å), Phe416Cε2(3.5 Å), Val417Cγ2(4.0 Å)
C8	Phe416Cε2(3.5 Å), Phe416Cζ(4.1 Å)
C9	Ile265δ1(4.0 Å), Phe416Cε2(3.8 Å), Phe416Cζ(4.1 Å)
C10	Val105Cγ1(4.5 Å), Ile265δ1(3.5 Å), Phe416Cζ(4.1 Å)
C11	Thr273Cγ2(4.0 Å), Phe416Cε2(3.9 Å), Val417Cγ2(3.2 Å)
C12	Asp272Cβ(4.6 Å), Val417Cγ1(4.4 Å) Val417Cγ2(3.5 Å)
C13	Phe190Cβ(3.9 Å), Phe416Cε2(4.2 Å)
C14	Phe190Cβ(3.8 Å), Ser268Cβ(3.6 Å), Phe416Cε2(3.9 Å)

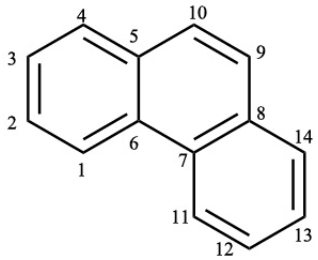

Table S5. Comparison of different proximal face residues of CYP108D1 to those of CYP101A1, CYP101D1, CYP101D2, CYP101C1 and CYP108A1.

CYP108D1	CYP101A1	CYP101D1	CYP101D2	CYP101C1	CYP108A1
Lys67	Glu76	Arg77	Ser76	Gly61	Lys65
Lys114	Gln110	Pro111	Pro110	Ala95	Ala112
Arg117	Ala113	Lys114	Lys113	Thr98	Gly115
Asp121	Gln117	Lys118	Lys117	Lys102	Asn119
Lys126	Pro122	Ala123	Ala122	Arg107	Ala124
Gln378	Leu356	Arg363	Arg362	Arg343	Met376
Arg390	Ile368	Thr375	Ile374	Ile355	Lys388

Figure S1 (a) SDS-PAGE and (b) UV/Vis spectra of purified CYP108D1 used for X-ray crystallography.

(a)

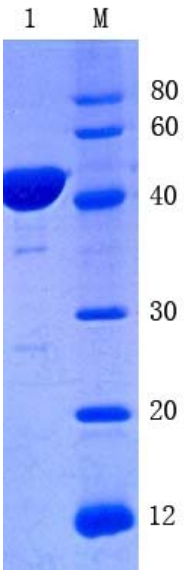

(b)

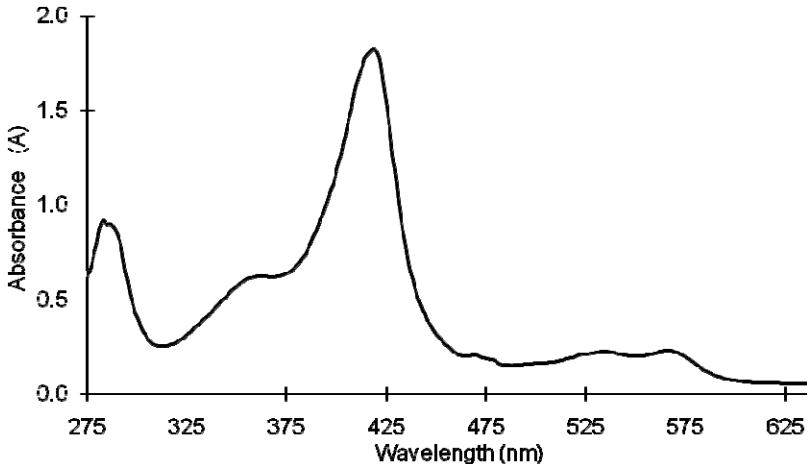

Figure S2 Secondary structure comparison between CYP108D1 (green) and CYP108A1 (PDB code: 1CPT) (cyan). The β-sheet 1-5, the β4 (β4-1, β4-2) and β5 sheets (β5-1, β5-2) in CYP108A1 are disordered loops in CYP108D1 (red). As a result the β3-2 and β4-2 sheets which merge in CYP108A1 are much shorter in CYP108D1.

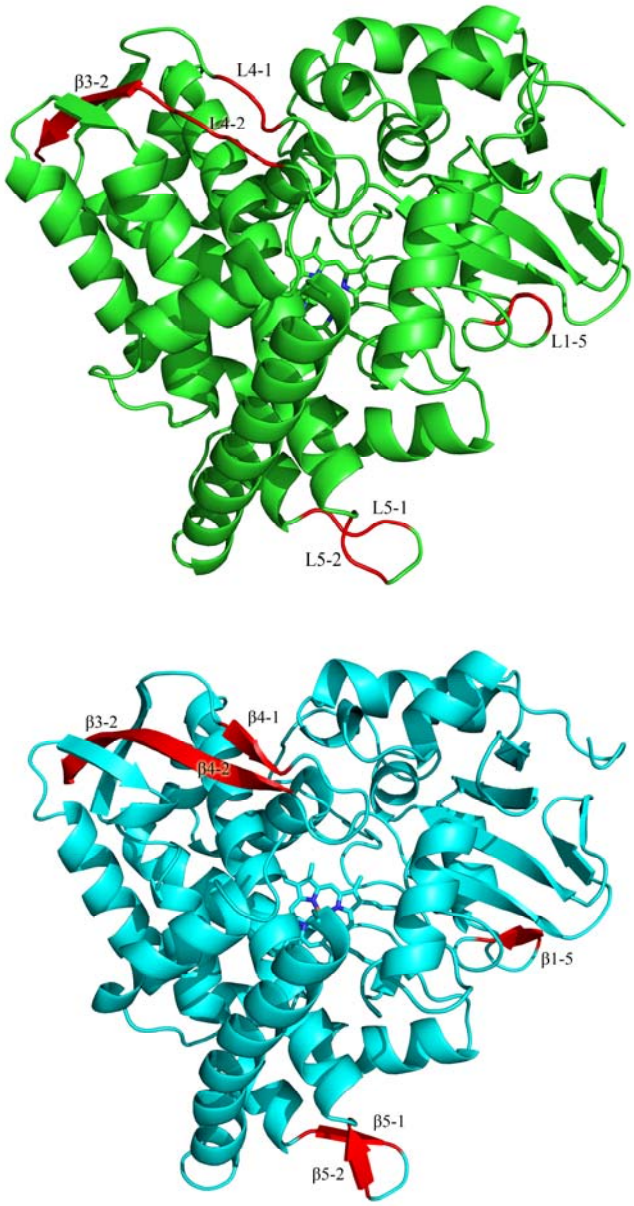

Figure S3 Sequence alignment of CYP108D1 with CYP108A1. Black arrows and cylinders indicate the β-sheets and α-helices, respectively. Conserved residues are highlighted. Residues in the active site are labeled with red triangles.

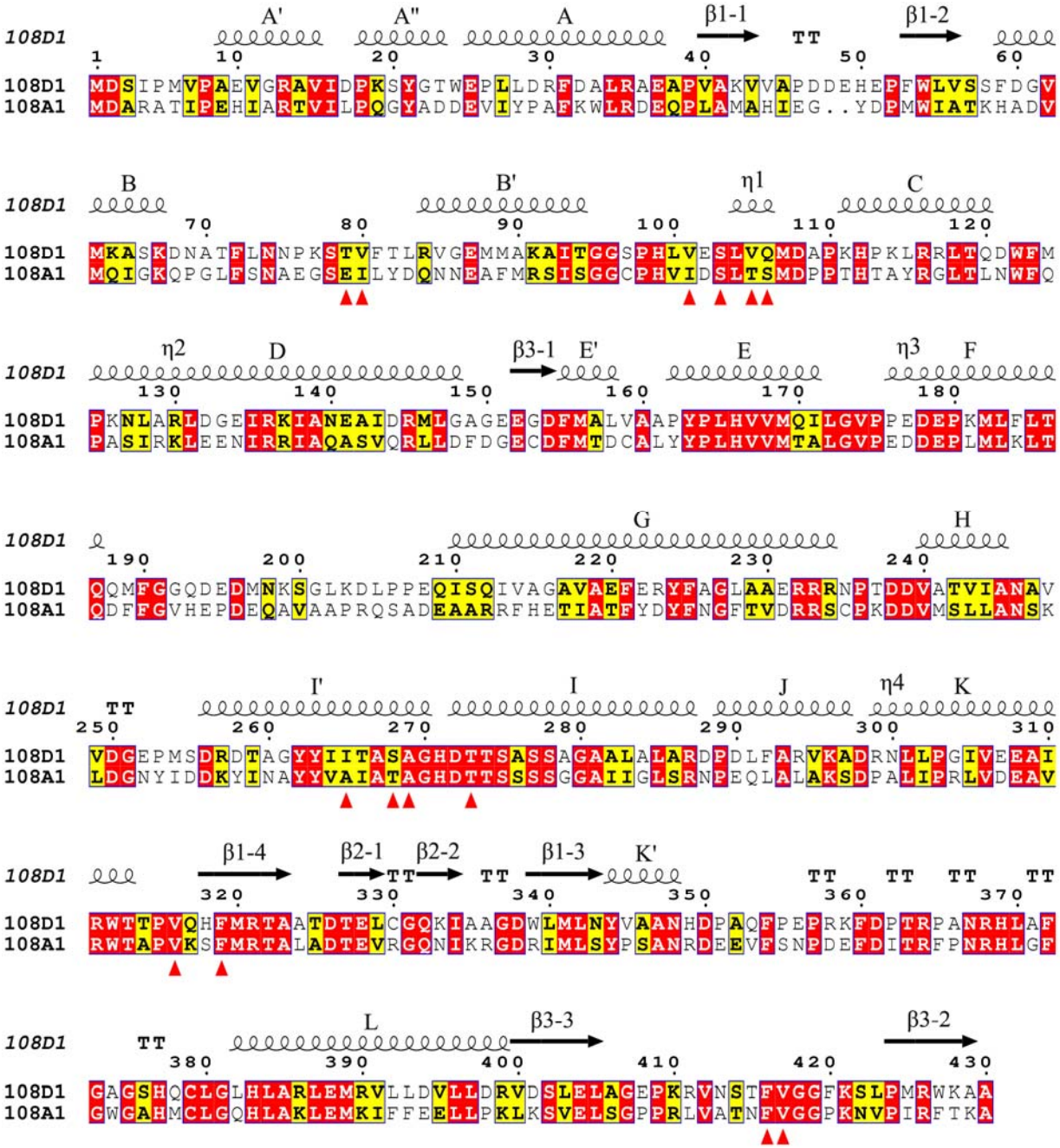

Figure S4 The r.m.s.d. plot of CYP108D1 versus CYP108A1.

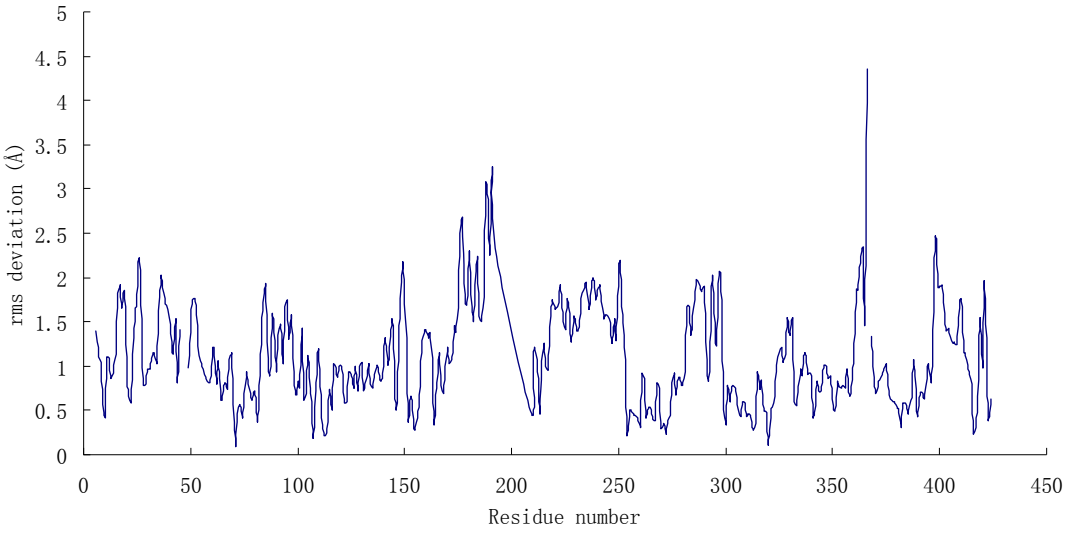

Figure S5 Comparison of the active site residues of CYP108D1 (green) and CYP108A1 (gray). The heme of CYP108D1 is shown in yellow and residue differences in CYP108A1 are highlighted in brackets.

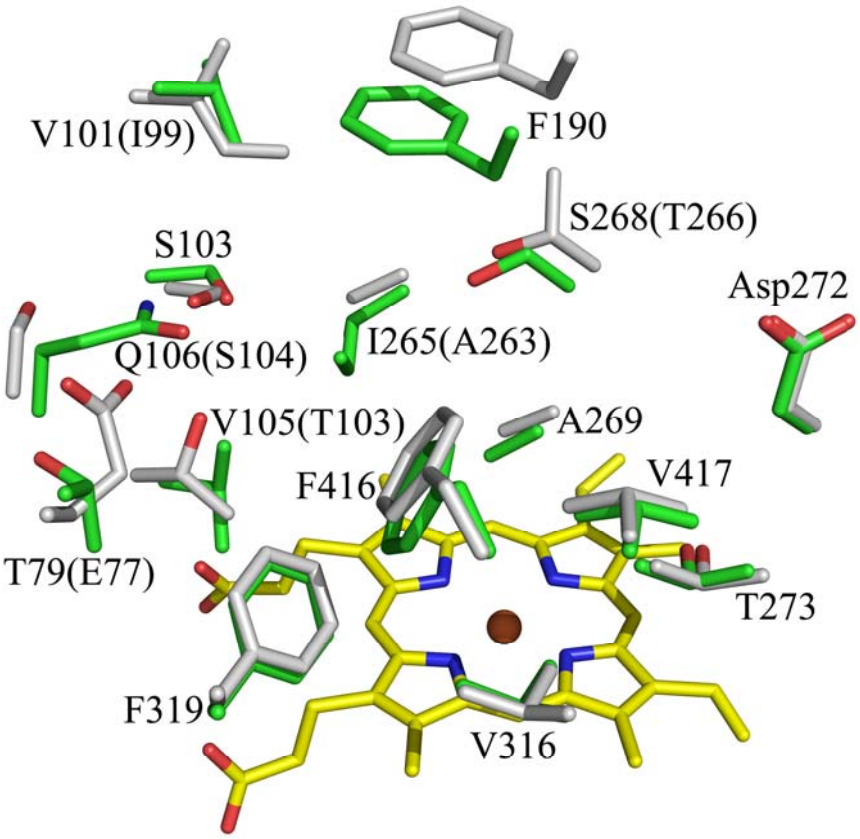

Figure S6 UV/Vis spectra of ferric CYP108D1 (red), reduced CYP108D1 (blue) and reduced-CO bound CYP108D1(black).

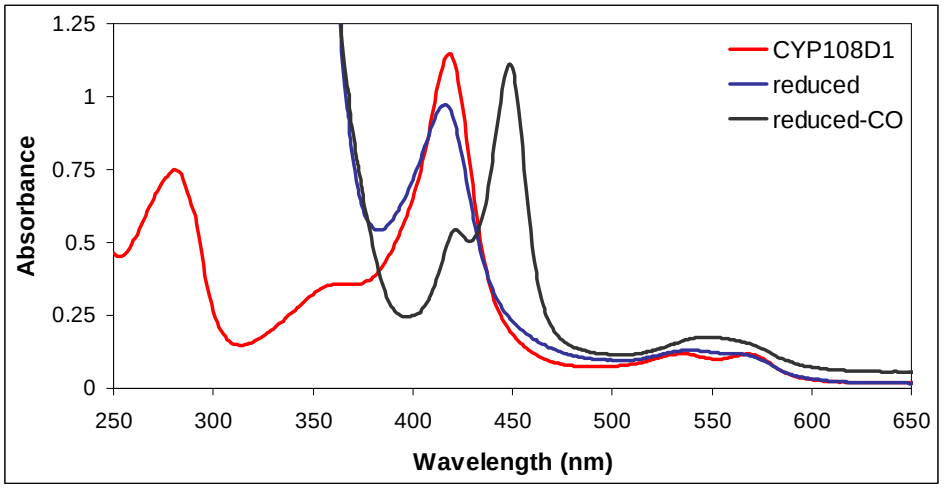

Figure S7 The potential short path for proton delivery in CYP108D1. A chain of water molecules leads from the protein surface to the OD2 atom of Asp272 which is hydrogen bonded to the only water molecule above the I-helix groove (Wat37).

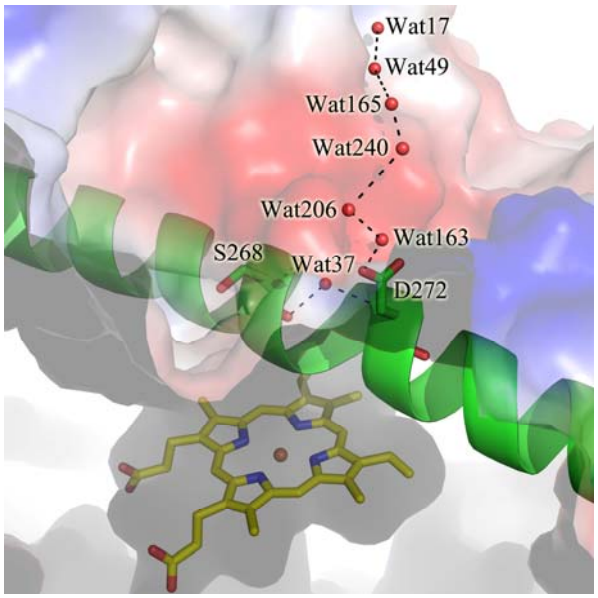

Figure S8 Spin state shifts of CYP108D1 with (a) phenylcyclohexane, (b) phenanthrene, (c) Biphenyl and (d) fluorene, napthalene and diphenylmethane.

(a)

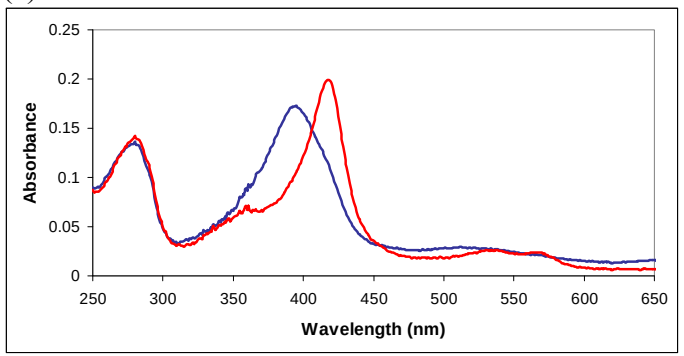

(b)

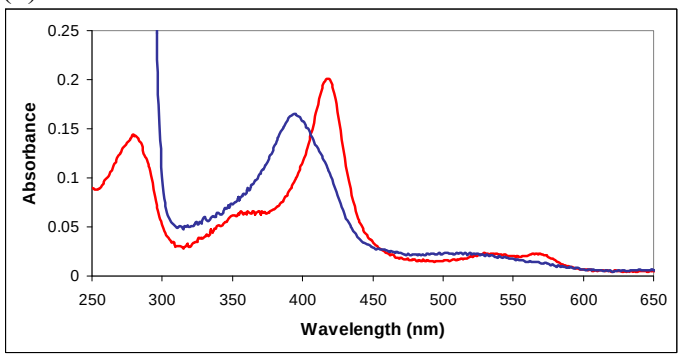

(c)

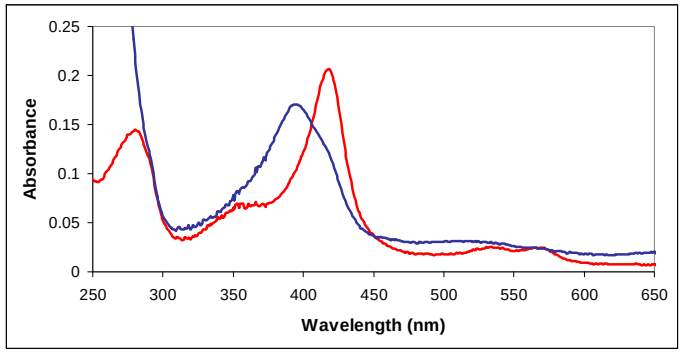

(d)

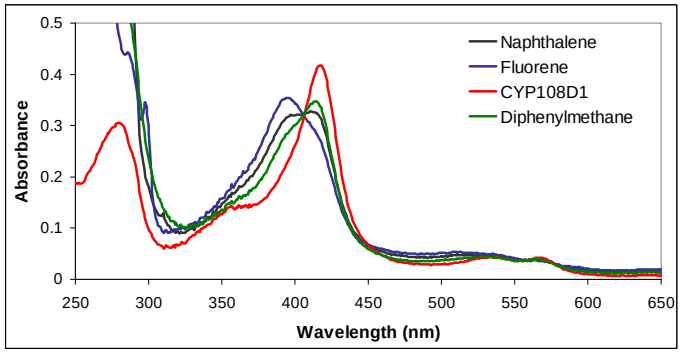

Figure S9 Substrate binding titrations for CYP108D1 with (a) α-terpineol, (b) fluorene and (c) naphthalene

(a)

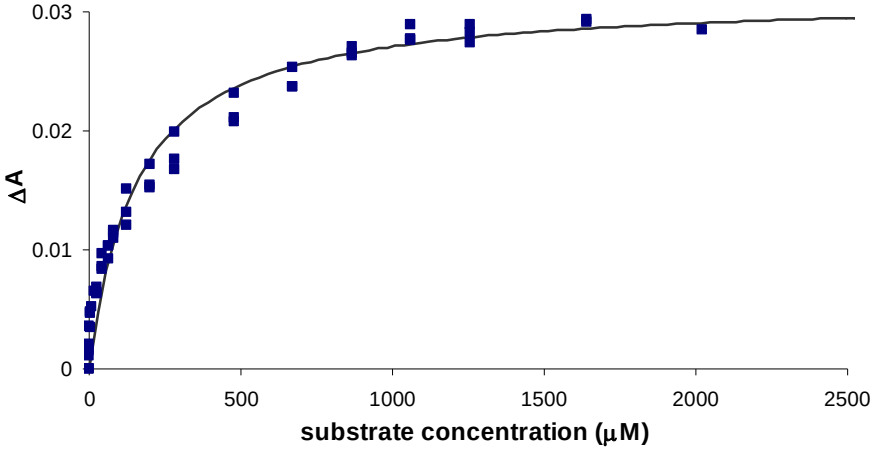

(b)

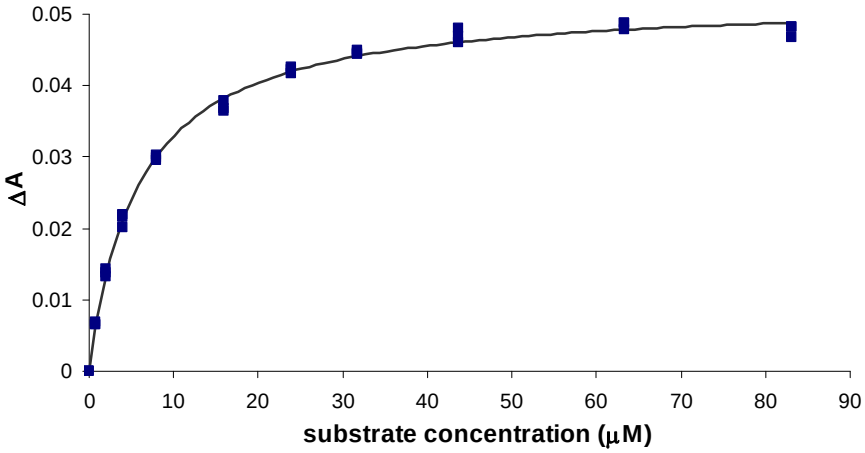

(c)

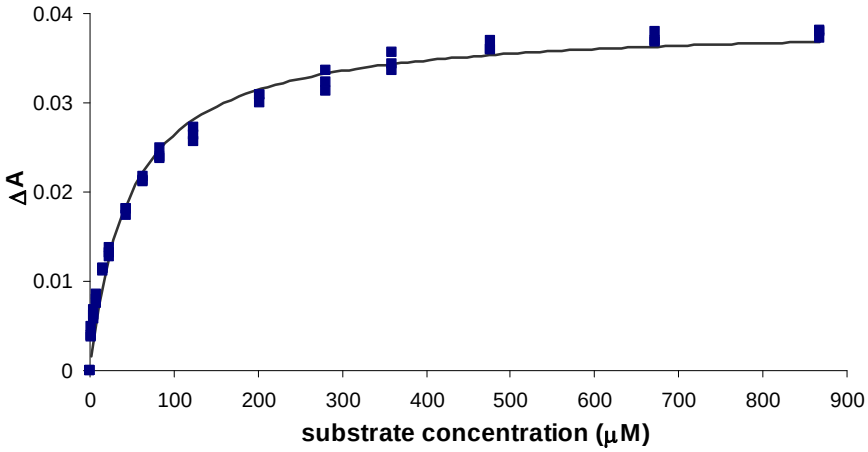

Figure S10 Phylogenenetic tree of the CYP108 family. CYP108D1 is at the bottom with three other members of the CYP108D subfamily from *Erythrobacter* species. CYP108A1 (P450terp) is clustered with the other members of the CYP108A family from *Frankia* sp. and *Rhodoccocus opacus* bacteria. The remaining CYP enzymes belong to the CYP108B family with the exception of one member of the CYP108E family from *Ralstonia metallidurans* (which has since been renamed *Cupriavidus metallidurans)*. The data was taken from the CYP450 engineering database (http://www.cyped.uni-stuttgart.de/) and the phenogram generated at Phylodendron (http://iubio.bio.indiana.edu/treeapp/treeprint-form.html).

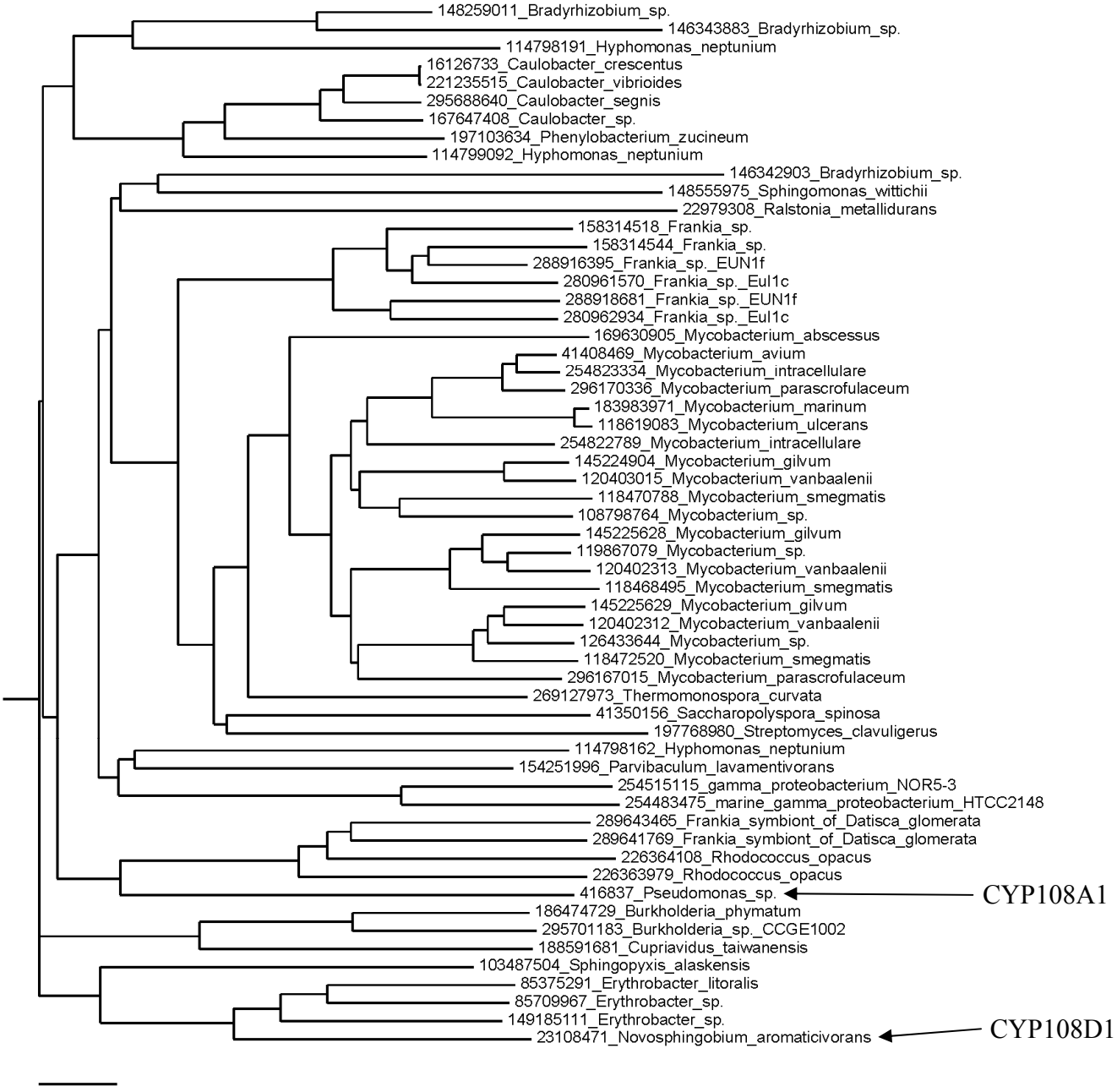

Figure S11 EPR spectra of (a) substrate free (black) and phenylcyclohexane bound (red) CYP108D1. The spectra were recorded using a microwave frequency of 9.3908 GHz and the magnetic field strength in mT is shown on the axis. The inset focuses in on the region at ~80 mT where one would expect to observe a peak if a high spin component was present and (b), substrate free (black) and camphor bound (red) CYP101A1.

(a)

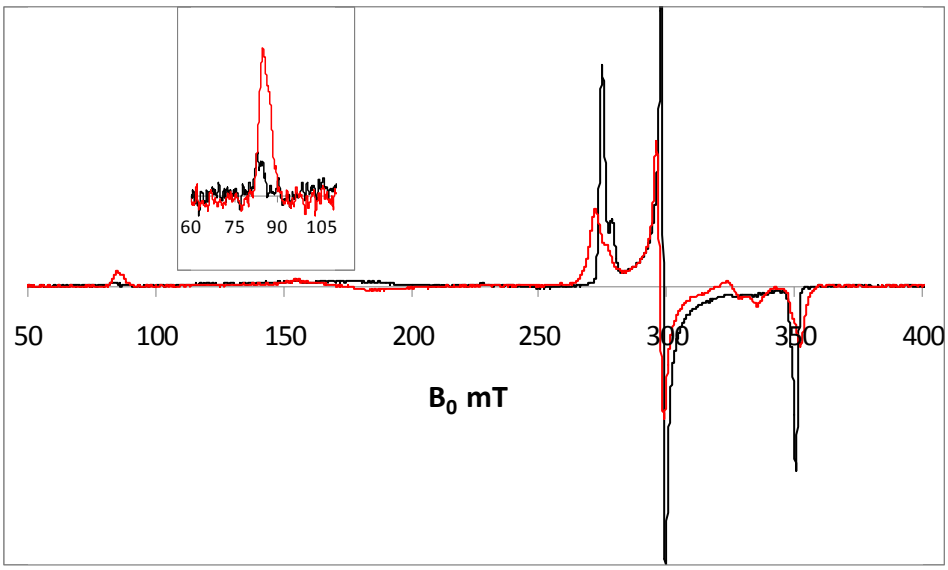

(b)

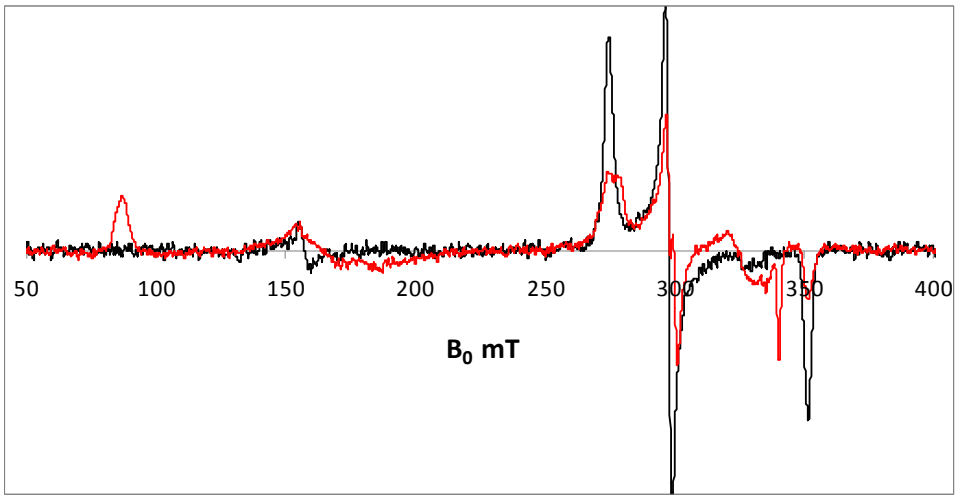

Figure S12 (a) The two lowest energy orientations of phenylcyclohexane in CYP108D1 calculated using AutoDock. The two phenylcyclohexane molecules are shown in blue (mode 1) and salmon (mode 2). Val105, Phe190, Ile265, Ala269, Thr273, Val316, Phe319, Phe416 and Val417 are in van der Waals contact with the phencyclohexane molecules (Table S3).

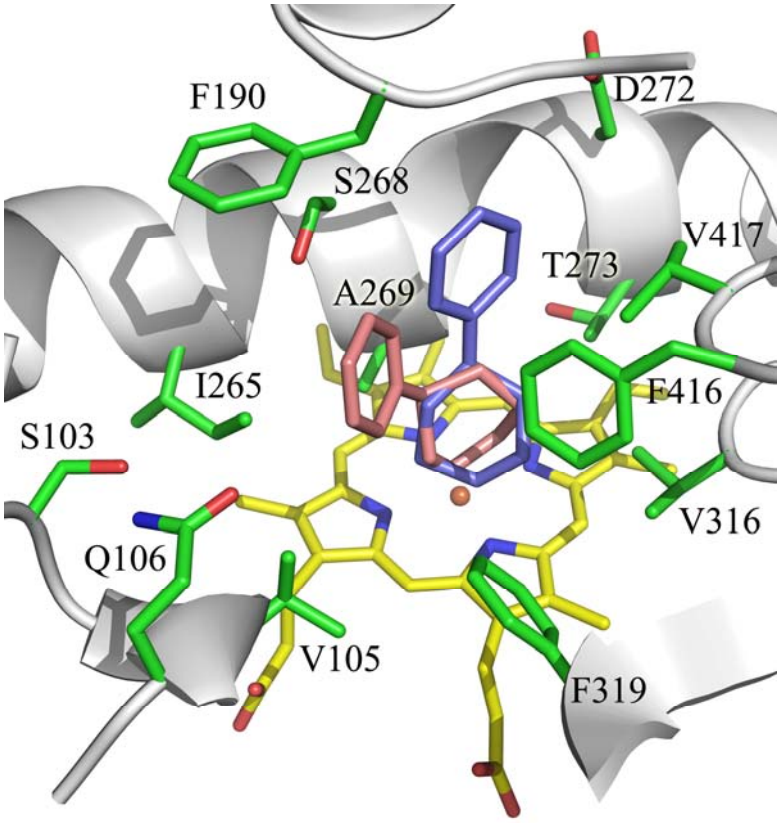

In both modes the phenyl ring interacts with the side-chains of Phe190 and Phe416. In the first mode the phenyl ring interacts with Val417, the Cβ of Asp272 and the Cα of Phe190 (Fig. 3b and Table S3). In the second mode the molecule is tilted and the phenyl ring moves towards Ile265 and the phenyl ring of Phe190 (Fig. 3b). In both modes the aliphatic cyclohexyl ring is nearest to the heme with the C4 carbon being the closest to the heme iron. The Fe–C distances were 4.0 Å and 4.5 Å, and the C–Fe–S angles were 158° and 151°, respectively. The cyclohexyl ring carbons were in hydrophobic contact with Val105, Ala269, Thr273, Val316 and Phe319.

(b) The lowest energy orientation of phenanthrene in CYP108D1 calculated using AutoDock. Phenanthrene is shown in salmon. Val105, Phe190, Ile265, Ala269, Thr273, Val316, Phe319, Phe416 and Val417 are in van der Waals contact with the phenanthrene molecule (Table S4).

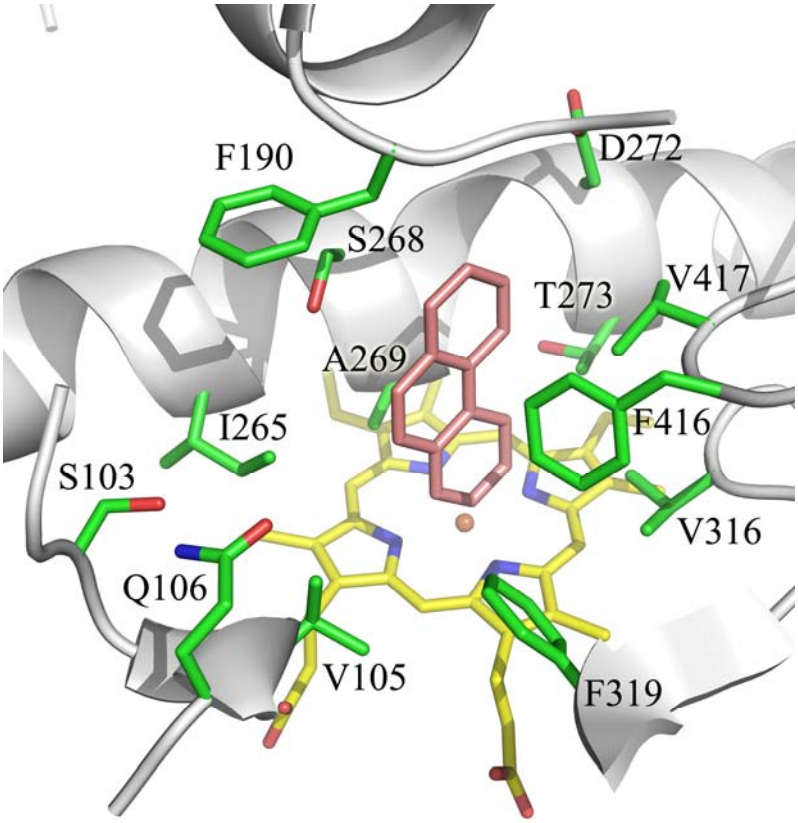

The three rings of phenanthrene contact Val105, Ile265, Ala269, Thr273, Val316, Phe319, Phe416, and Val417 and are removed from any polar residues in the active site (Fig. 3c and Table S4). The closest carbon of phenanthrene to the heme iron is the C2 carbon, at a Fe–C distance of 4.0 Å with a C–Fe–S (Cys379) angle of 156°.

Figure S13 GC coelution experiments (a) CYP108D1 with phenylcyclohexane (blue), 4-phenylcyclohexanone (black), 4-phenylcyclohexanone reduced with NaBH4 (green) and CYP101A1 (Y96F/V247L mutant) with phenylcyclohexane (red). (b) CYP108D1 with *p*-cymene (black), carvacrol (blue), thymol (green), *p*-α,α-trimethylbenzyl-alcohol (red) and 4-isopropylbenzylalcohol (grey dashes). (c) CYP108D1 with α-terpineol (blue), α-terpineol (red) and β-pinene oxide reacted with $Hg(NO_3)_2$ to yield 7-hydroxyterpineol.

(a)

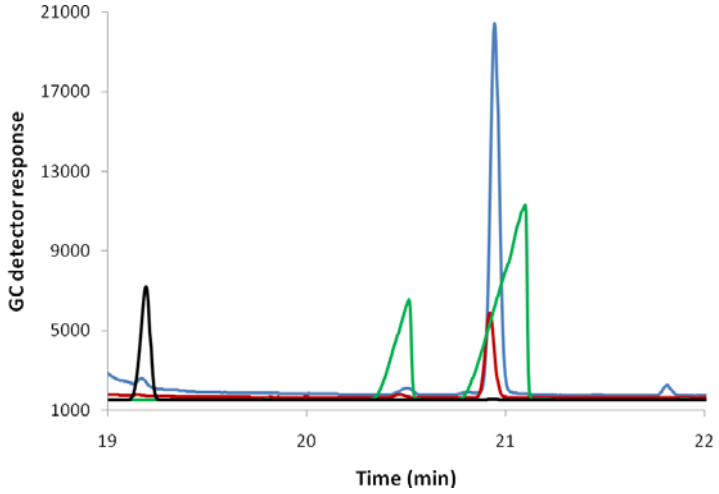

(b)

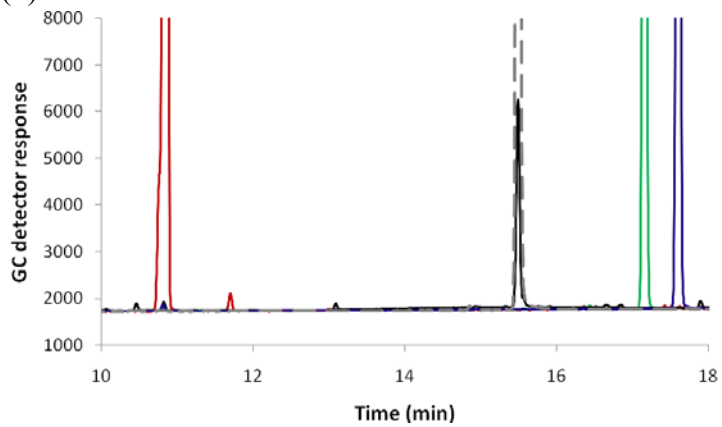

(c)

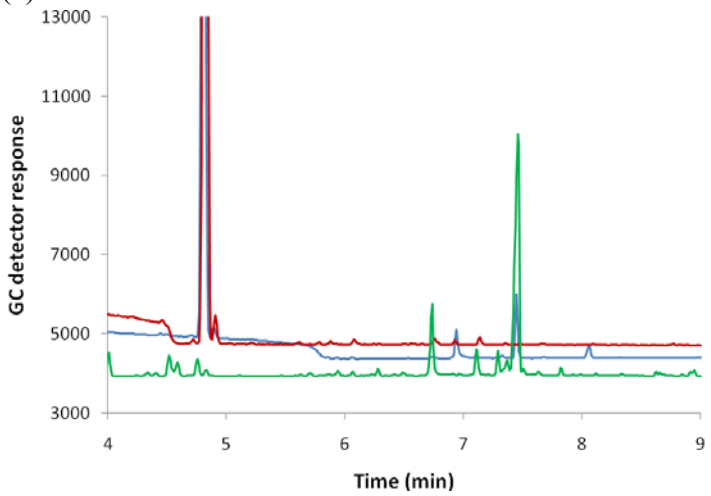

Figure S14 (a) Electrostatic potential of the proximal face of **A** CYP101A1, **B** CYP101D1, **C** CYP101D2, **D** CYP101C1 and **E** CYP108A1

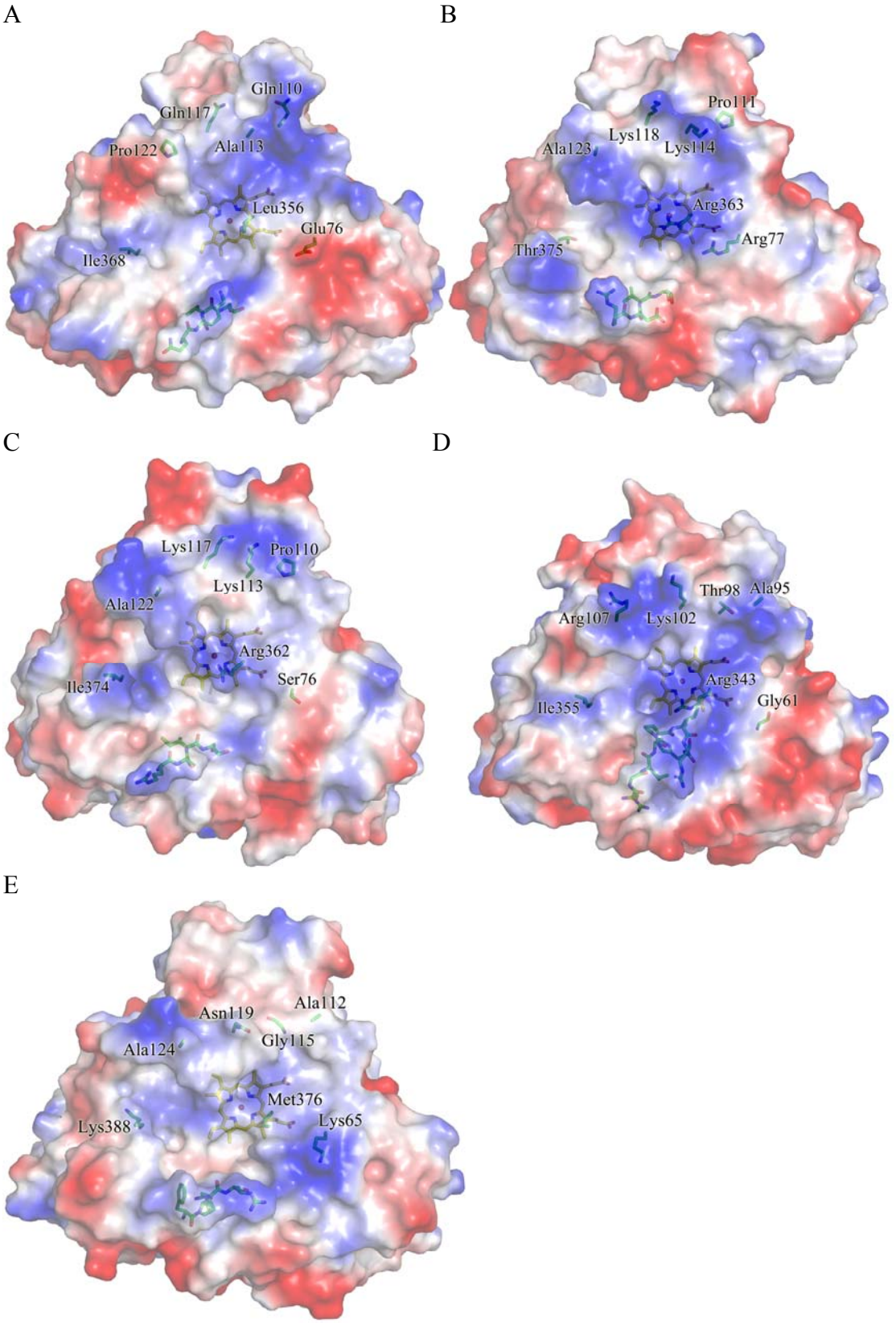

Figure S14 (b) The orientation of the loop region from residue Pro365 to Arg368 (shown in magenta) in **A** CYP108D1, **B** CYP108A1, **C** CYP101A1, **D** CYP101C1, **E** CYP101D1, **F** CYP101D2. The loop differs significantly from the other structurally characterised CYP enzymes and leads to a different topology of the proximal face. The proximal loop (blue) and the heme (yellow) also shown for orientation purposes.

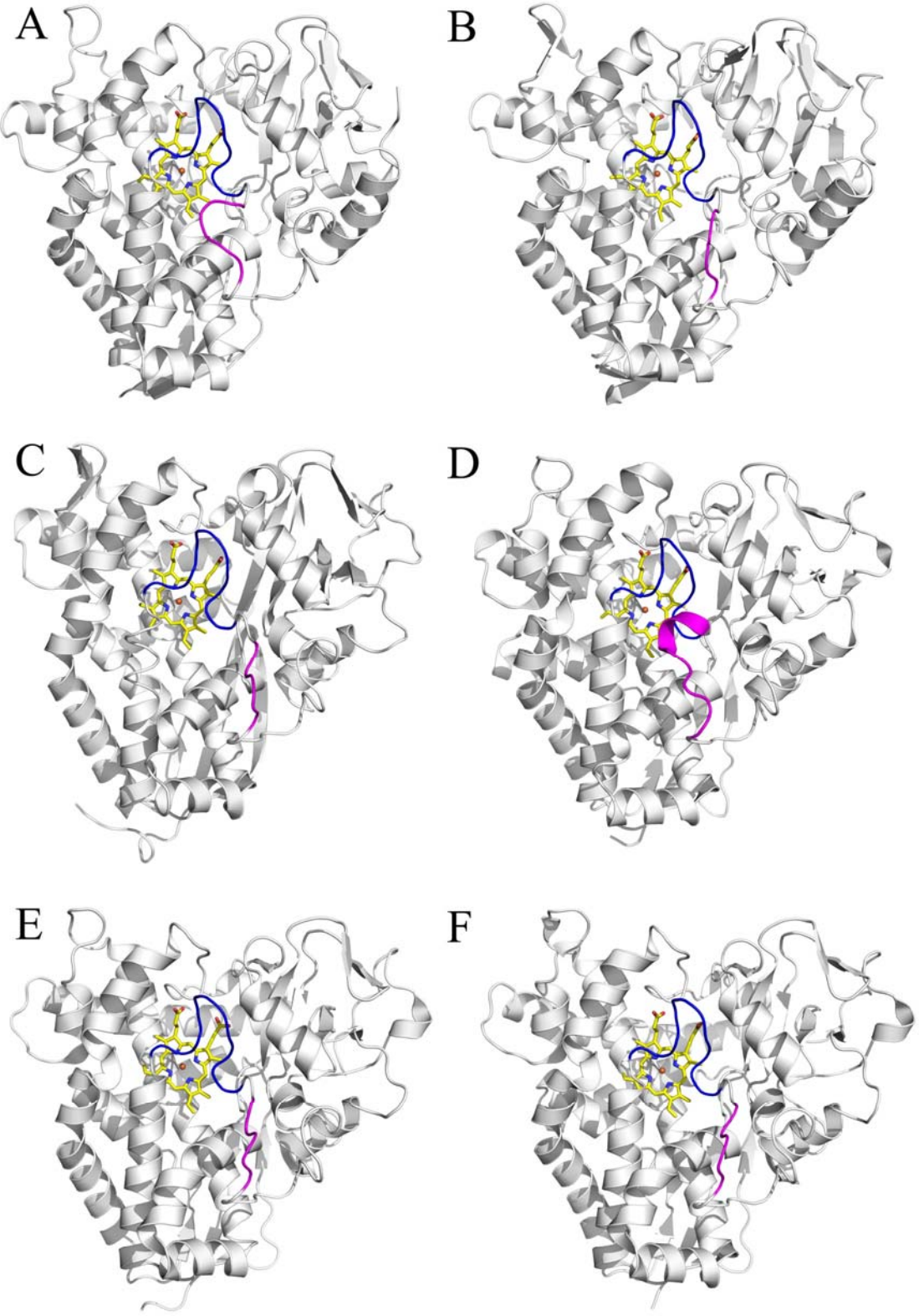

Figure S15 (a) The active site volume of CYP108D1 as calculated by VOIDOO. The two docking modes of phenylcyclohexane are also shown (see Fig. S12a). The secondary structure of the protein is also included for reference.

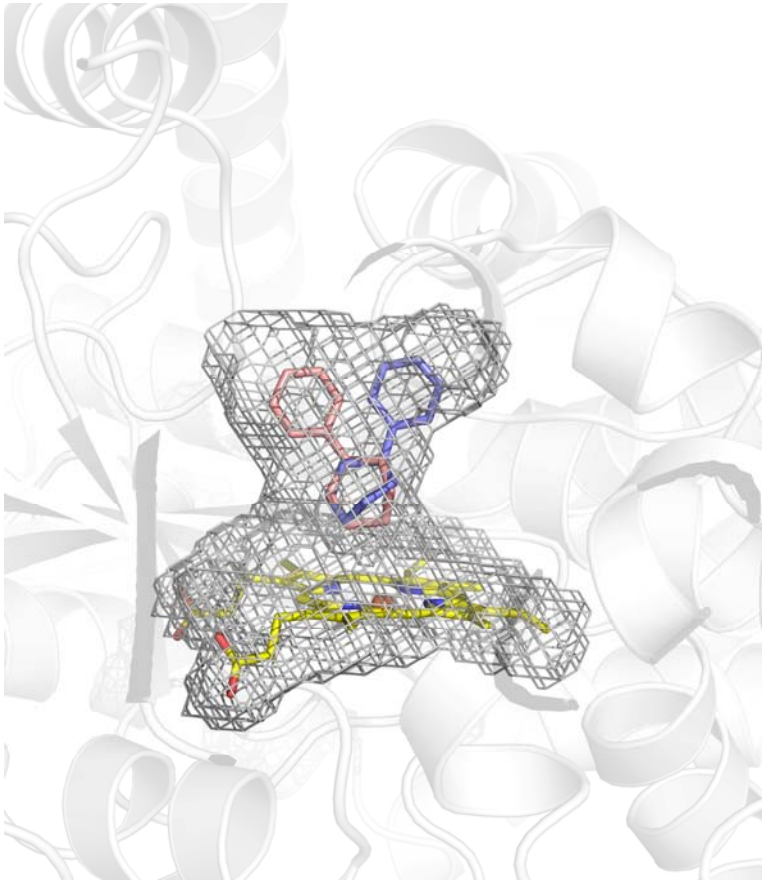

Figure S15 (b) The active site volume of CYP108D1 as calculated by VOIDOO. The docking mode of phenanthrene is also shown (see Fig. S12b). The secondary structure of the protein is also included for reference.

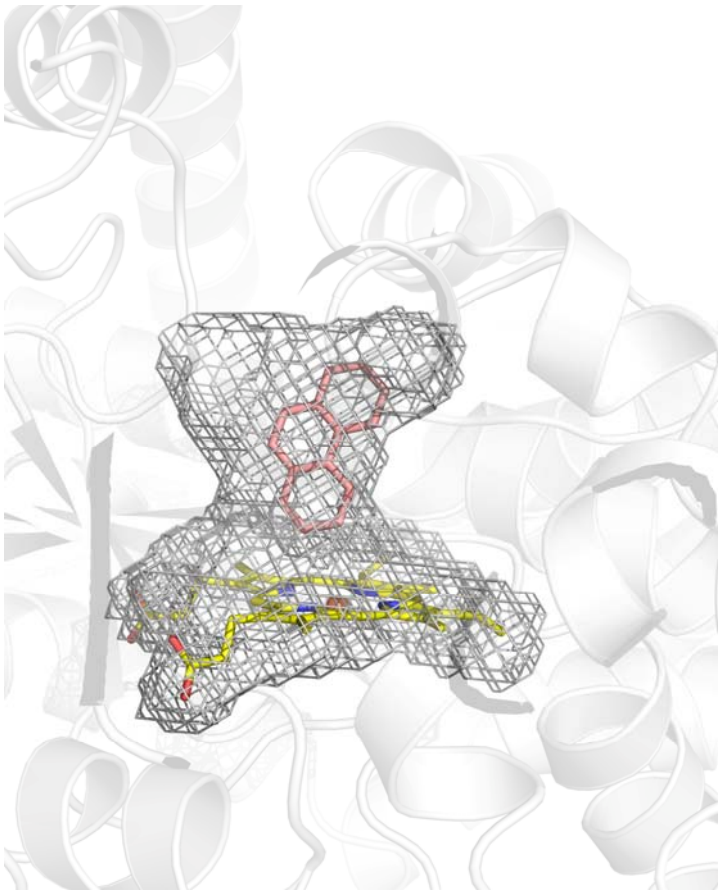

Figure S16 (a) Time courses for $Fe^{II}(CO)$ complex formation monitored at 450 nm for camphor bound CYP101D1 (red) and phenylcyclohexane bound CYP108D1. Final concentrations of 1 µM P450 and 2.5 µM Arx were used in these examples. (b) The fitting (red) of the initial phase of camphor bound CYP101D1 (black) to a single exponential. The rate constant was 22.9 ± 0.8 s^{-1}. The residuals of the fitting are shown as an insert.

(a)

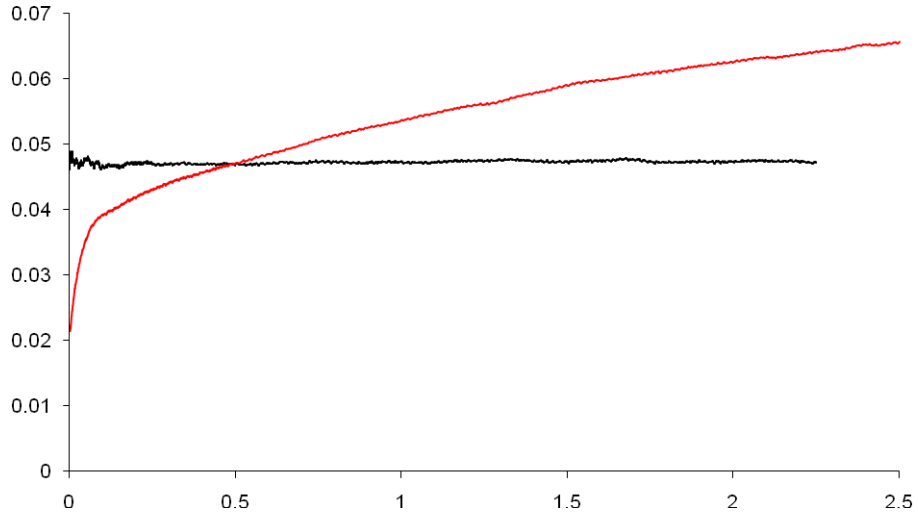

(b)